Automated Modal Analysis of Entanglement with Bipartite Self-Configuring Optics

Charles Roques-Carmes,*,† Aviv Karnieli,*,† David A. B. Miller, and Shanhui Fan*
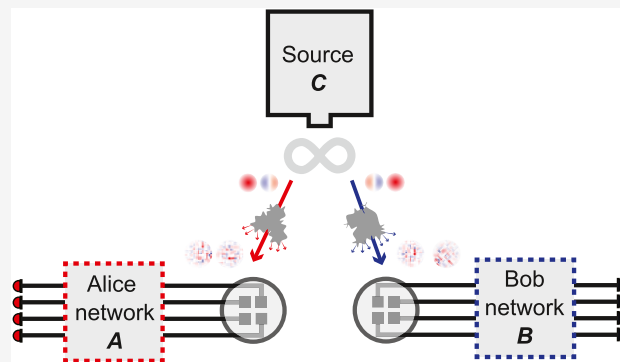
Read Online

ACCESS | Metrics & More | Article Recommendations | Supporting Information

ABSTRACT: Entanglement is a unique feature of quantum mechanics. In coupled systems of light and matter, entanglement manifests itself in the linear superposition of multipartite quantum states (e.g., parametrized by multiple spatial, spectral, or temporal degrees of freedom of a light field). In bipartite systems, the Schmidt decomposition provides a modal decomposition of the entanglement structure over independent, separable states. Although ubiquitous as a mathematical tool to describe and measure entanglement, there exists no general efficient experimental method to decompose a bipartite quantum state onto its Schmidt modes. Here, we propose a method that relies on bipartite self-configuring optics that automatically "learns" the Schmidt decomposition of an arbitrary pure quantum state. Our method is designed for entanglement distributed over spatial or spectral degrees of freedom of a light field and can reconstruct the Schmidt modes and values by variational optimization of the network's output powers or coincidences. We illustrate our method with numerical examples of spectral entanglement analysis for biphotons generated via spontaneous parametric down conversion and provide experimental guidelines for its realization and generalization to other degrees of freedom of light, including the influence of losses and impurities. Our method provides a versatile and scalable way of analyzing entanglement in bipartite integrated quantum photonic systems.

KEYWORDS: *integrated photonics, spontaneous parametric down conversion, entanglement, quantum teleportation, reconfigurable optics*

INTRODUCTION

Entanglement is a fundamental property of quantum mechanical systems,[1] underpinning quantum computing algorithms,[2] cryptography,[3] teleportation protocols,[4] and tests of nonlocal realism.[5,6] Optics is a prime platform for the generation and manipulation of entanglement between the many degrees of freedom of light and matter systems.[7−10] A paradigmatic example of bipartite entangled states in optics is photon pairs generated via spontaneous parametric down conversion (SPDC), which have been the workhorse of quantum photonic logic, computing, and simulations.[11−14] There has been a growing interest in controlling the entanglement of photon pairs with engineered pumps and nonlinear crystals.[15−19] Such engineered quantum sources may be used to shape separable biphoton wave functions for heralding[20−22] and for quantum information processing.[19,23,24]

A successful implementation of quantum computing and simulation protocols entails an accurate description and characterization of entanglement. In pure bipartite quantum systems, measures of entanglement are provided by the Schmidt number and the von Neumann entropy.[1] Generally, the Schmidt decomposition of a pure bipartite state provides a convenient modal description of entanglement (as a linear superposition of separable and orthogonal "Schmidt modes").[25,26] Performing the Schmidt decomposition becomes progressively challenging as the Hilbert space becomes larger and even continuous, as in the case of encoding quantum entanglement in the spatial and spectral correlations of photon pairs.[19,23,24,26,27]
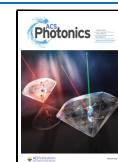
The problem of efficient Schmidt decomposition is an active field of study,[28−32] important for applications such as high-dimensional quantum communication[28,33−35] and quantum imaging.[36,37] Assumptions on the spatial and spectral shape and symmetries of the driving pump field and nonlinear crystal in SPDC can approximate the Schmidt decomposition analytically[26,30−32,38−43] and reduce the scaling of the number of required measurements.[28,29] However, to date, there is no efficient method for measuring the Schmidt decomposition in the most general setting of high-dimensional entangled photon states.

Programmable networks of Mach−Zehnder interferometers (MZIs)[44,45] are an ideal platform for integrated quantum photonics.[8] They have enabled the realization of quantum key distribution,[46] variational quantum algorithms,[47,48] multidimensional and multiphoton entanglement processing,[49,50] and quantum walk simulators.[51] In these demonstrations, the enabling feature of programmable MZI networks is that they can impart arbitrary unitary operators on spatial modes of quantum optical states.[11,52,53]

Self-configuring programmable network architectures[52−61] additionally offer simple and progressive configuration of the MZIs based only on power minimizations or maximizations, adapting automatically to the problem of interest, sometimes even without calculations. They can learn modal representations of (quantum) optical fields (e.g., communication modes[54,55,60] and natural modes of partially coherent light[61]). However, their potential in the modal analysis of entanglement in bipartite quantum optical systems has not been explored thus far.
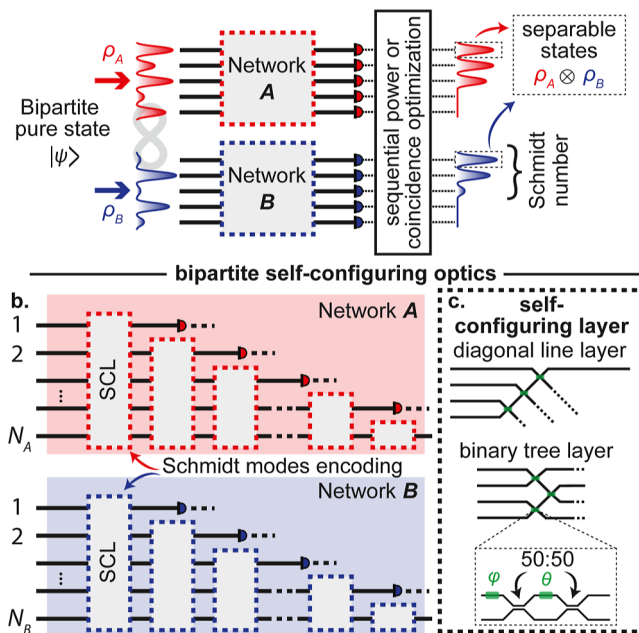
Here, we propose a method to automatically analyze entanglement in bipartite quantum optical systems using self-configuring optics. Our approach relies on bipartite self-configuring networks (BSCNs) composed of MZI meshes that impart unitary transformations over spatial modes of the two subspaces of the bipartite system. The average power or coincidence counts at the output of the BSCN are sequentially optimized, which results in the network having "learned" the Schmidt decomposition of an input state. Then, the Schmidt number can be directly measured at the output (as the number of ports with nonzero average power/coincidence), and the Schmidt modes of the system can be deduced directly from the network's settings. Our approach automatically discovers the Schmidt modes without presuming any prior knowledge about these modes. Furthermore, our architecture sequentially learns the most important Schmidt modes first (corresponding to the largest Schmidt values). In the practically important case where only a few Schmidt modes dominate, our method offers favorable linear scaling with the Hilbert space dimension, both in required physical hardware and in the number of iterations (optimization updates), compared to the quadratic scaling associated with reconstructing an entire density matrix to perform a Schmidt decomposition.

While our method is naturally designed to process entanglement in the spatial domain, we propose ways to generalize it to other degrees of freedom of light (spectral, polarization, etc.). We first illustrate our method with numerical examples in the spectral domain of photon pairs generated via SPDC. We show that our method can automatically measure Schmidt modes of photon pairs while being robust to single-photon losses. Since our method allows us to automatically learn a modal decomposition of entanglement in the system, we also discuss potential applications in modal shaping of separable light, generation of states with controlled entanglement, and entanglement distribution protocols for quantum communication through scattering media. Our method paves the way to characterization, processing, generation, and distribution of entanglement in quantum optical states. We envision that our approach could form a building block in integrated quantum optical architectures for computing and simulation where entanglement measurement and control play an essential role.

■ RESULTS

Automatic Schmidt Decomposition and Entanglement Analysis of Bipartite Quantum Optical Systems with Self-Configuring Optics.
We consider a pure state input $|\psi_{in}\rangle$ to the BSCN of Figure 1 (later, we shall consider

Figure 1. Automatic Schmidt decomposition of bipartite quantum optical systems with self-configuring optics. (a) Conceptual schematic of automatic Schmidt decomposition enabled by bipartite self-configuring optics. A bipartite pure state $|\psi_{in}\rangle$ is input to two networks A and B acting upon Hilbert spaces H_A and H_B, respectively. Their outputs (either power or coincidence counts) are sequentially optimized. The resulting output is a linear superposition of orthogonal separable states (Schmidt decomposition), and the Schmidt number can be read off as the number of nonzero outputs. (b) Bipartite self-configuring network (BSCN) architecture. Each network consists of a cascade of self-configuring layers (SCLs). Each such SCL separates one mode to its output port (here, the top one in each layer), passing the remaining field to the next layer. (c) SCL architecture, consisting of, e.g., a diagonal line or binary tree layer. Each node corresponds to a 2 by 2 Mach−Zehnder interferometer (MZI) parametrized by phases (φ, θ).

photonic losses that might impair the state's purity). The input state is bipartite and is defined over the tensor product of two Hilbert spaces, H_A and H_B, with dimensions N_A and N_B, respectively. These dimensions can be large and even cover the (discretized) case of a continuous Hilbert space, e.g., as in spectral-bin encoding.[24,62] A concrete example of this model consists of two single photons propagating over spatial modes of integrated networks A (red) and B (blue). We can decompose the state over an orthogonal basis $|x_j\rangle_A|x_k\rangle_B$ of $H_A \otimes H_B$ and write its Schmidt decomposition as

$$|\psi_{in}\rangle = \sum_{jk} G_{jk}|x_j\rangle_A|x_k\rangle_B \tag{1}$$

$$= \sum_{i=1}^{r} \lambda_i|y_i\rangle_A|y_i\rangle_B \tag{2}$$

where G is a $N_A \times N_B$ state matrix whose singular value decomposition $G = UDV^\dagger$ maps to the input state's Schmidt decomposition[63] as $|y_i\rangle_A = \sum_j U_{ji}|x_j\rangle_A$, $|y_i\rangle_B = \sum_j V_{ki}^*|x_k\rangle_B$, and $D_{ii} = \lambda_i$ are the r singular values of G (ordered by the decreasing value $\lambda_1 \geq \cdots \geq \lambda_r > 0$). As can be seen from eq 2, the Schmidt decomposition provides a modal description of entanglement as a linear superposition of mutually orthogonal and separable states. The Schmidt number r, which quantifies the amount of entanglement in the state, corresponds to the number of nonzero λ_i's. The Schmidt decomposition directly yields the von Neumann entropy of the input state: $S = -\sum_k \lambda_k^2 \log(\lambda_k^2)$.

The network shown in Figure 1 can automatically perform Schmidt decomposition of an input state $|\psi_{in}\rangle$ by simultaneous diagonalization of the reduced density operators of each subspace. The network is made of two cascades of self-configuring layers (SCLs) that form networks A and B (see Figure 1b). SCL architectures can be defined topologically;[56] each SCL has a single output that is connected to each input by only one path through the MZI blocks. (Other unitary architectures could be used for these layers, but SCLs support simple configuration and have the minimum number of programmable elements.)

These SCL cascades operate on spaces H_A and H_B, respectively, transforming their reduced density matrices as $\rho^A \to U^A \rho^A (U^A)^\dagger$ and $\rho^B \to U^B \rho^B (U^B)^\dagger$, where U^A and U^B are reconfigurable unitary matrices imparted by networks A and B, respectively. This SCL architecture allows for the implementation of sequential, layer-by-layer optimization methods.[52,53,61] Example SCL architectures include diagonal lines or binary trees of MZIs,[56] as shown in Figure 1c. These sequential, layer-by-layer optimizations over parameters of the BSCN can be realized by dithering[55,57] or in situ back-propagation.[58,64]

We now show how the BSCN of Figure 1 can learn the Schmidt decomposition of the input state $|\psi_{in}\rangle$. Sequential optimization of the average output powers measured at port k, $\langle P_k^A\rangle$ ($k = 1, ..., N_A$) and $\langle P_k^B\rangle$ ($k = 1, ..., N_B$) maps to a variational definition of the eigendecomposition of $GG^\dagger$ and $(G^\dagger G)^T$ (see Supporting Information (SM), Sections S1 and S2)

$$\max_{\tau_k^A}\langle P_k^A\rangle = \max_{u_k^A}(u_k^A)^\dagger(GG^\dagger)u_k^A = \lambda_k^2 \tag{3}$$

$$\max_{\tau_k^B}\langle P_k^B\rangle = \max_{u_k^B}(u_k^B)^\dagger(G^\dagger G)^T u_k^B = \lambda_k^2 \tag{4}$$

where τ_k^A (respectively, τ_k^B) are the parameters of the k-th self-configuring layer of network A (respectively, B) and u_k^A (respectively, u_k^B) the k-th column of $(U^A)^\dagger$ (respectively, $(U^B)^T$). One can see from eqs 3 and 4 that tracing out subspace B (respectively, A) allows for the variational definition of the left (respectively, right) singular vectors of G and their respective singular values.

Alternatively, sequential optimization of the single-photon coincidence counts between output ports k of networks A and B (where $k = 1, ..., \min(N_A, N_B)$) directly maps to a singular value decomposition of G (see SM, Section S2)

$$\max_{\tau_k^A, \tau_k^B}\langle C_{kk}\rangle = \max_{u_k^A, u_k^B}|(u_k^A)^\dagger G u_k^B|^2 = \lambda_k^2 \tag{5}$$

where the optimization runs over the k-th self-configuring layers of A and B simultaneously. Both optimization methods

will result in setting the network parameters to those of the Schmidt modes, corresponding to the singular value decomposition of G, such that $U^A = U^\dagger$ and $U^B = V^T$.

Both sequential optimization methods provide an automatic way to find the Schmidt decomposition of the input state $|\psi_{in}\rangle$. The resulting settings of the BSCN allow one to "read" the Schmidt modes (corresponding, for instance, to the decomposition of the complex joint spectral amplitude (JSA) of a biphoton state), and the Schmidt number corresponds to half the number of output ports with nonzero average power, or the number of output port pairs of the same index with nonzero coincidence. When considering two output ports sharing the same index k, $|x_k\rangle_A|x_k\rangle_B$, their joint output state is separable and corresponds to the amplitude of the Schmidt mode with the singular value λ_k. Individual Schmidt modes can be physically generated by feeding their corresponding output ports (while blocking the rest) as inputs to a pair of complementary networks applying $U_A^\dagger$ and $U_B^\dagger$ (as shown in Figure 4). A detailed derivation and description of the sequential optimization methods can be found in SM, Sections S1 and S2.
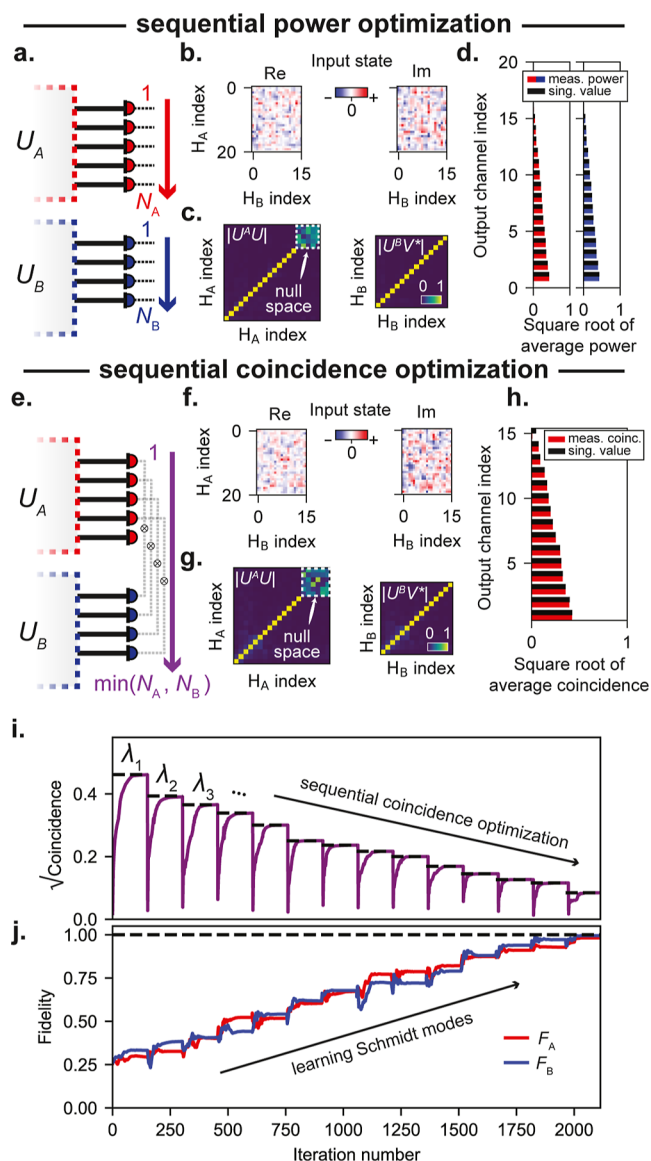
In the following, we turn to numerical examples illustrating our method, first with random matrices, to show the generality of this approach and then the experimentally relevant case of photon pairs generated via SPDC.

In this first numerical example, we consider the performance of the two sequential optimization methods mentioned in the previous section. In both cases, gradients are calculated via automatic differentiation and optimization is performed via stochastic gradient descent.[65] The power optimization method (Figure 2a) runs over output ports k of network A for $k = 1, ..., N_A$ and then k of network B for $k = 1, ..., N_B$. We simulate the performance of the sequential power optimization over the outputs of the BSCN on a random matrix (shown in Figure 2b). First, the network learns the singular vectors of the state matrix G: this can be seen by plotting $U^A U$ and $U^B V^*$, which are equal to the identity matrix (except on the null space, see Figure 2c). The corresponding singular values can be read as the square root of the average power on the output ports of networks A and B, as shown in Figure 2d. The performance of the sequential coincidence maximization is shown on a similar random matrix G in Figure 2e–h, where a similar performance is achieved, and the singular values can be measured as the square root of the average coincidence between ports $|x_k\rangle_A$ and $|x_k\rangle_B$. In these examples, the BSCN accurately identifies the Schmidt modes and values.

In our numerical simulations, optimization is performed with a modified version of stochastic gradient descent,[65] and the performance of the algorithm is shown in Figure 2i,j for the sequential coincidence optimization. Each sequential coincidence (from 1 to $\min(N_A, N_B)$) quickly converges to the corresponding singular value. The fidelity increases over each sequential optimization step and reaches values ≈ 1 in our numerical experiments (for both Schmidt vectors in A and B, see fidelity definition in the SM).

We now discuss the computational cost (in terms of both physical resources and number of iterations) for the BSCN to perform Schmidt decomposition (e.g., to find the Schmidt mode corresponding to the largest Schmidt value). Importantly, since both methods rely on Rayleigh quotient optimization, their convergence can be formally proven, as we show in the SM, Section S7. This variational formulation of entanglement modal analysis also lends itself to stochastic gradient descent methods that have advantageous convergence
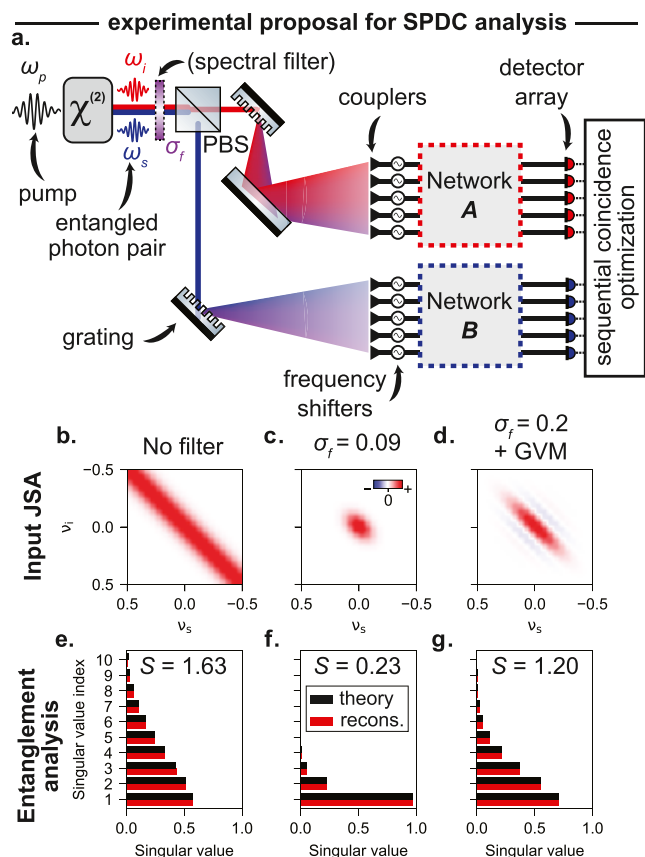
Figure 2. Sequential optimization methods for entanglement analysis in self-configuring optics. (a–d) Sequential power optimization. (a) Power optimization sequence: from 1 to N_A (on outputs of network A), then from 1 to N_B (on outputs of network B). (b) Random matrix input example. (c) Resulting eigenvector reconstruction from power optimization. (d) Resulting simulated square roots of power outputs (meas. power) and singular values (sing. values) at the outputs of networks A (red) and B (blue). (e–h) Sequential coincidence counts optimization. (e) Coincidence counts optimization sequence: from 1 to min (N_A, N_B) (on pairs of outputs ports from networks A and B). (f) Random matrix input example. (g) Resulting eigenvector reconstruction from coincidence optimization. (h) Resulting simulated square roots of coincidence counts (meas. coinc.) and singular values (sing. values). (i) Square root of coincidence over iteration number, mapping to their corresponding Schmidt values. (j) Fidelity of Schmidt modes in A (red) and in B (blue) over iteration number.

speeds (which can be essentially independent of the state's dimensionality in some implementations[66]). More generally, the number of iterations to achieve a given accuracy for a pair of Schmidt modes will scale like $O(N)$ (where N is the Hilbert space dimension), and we show this linear scaling in simulations in the SI, Section S7. Additionally, our method naturally orders the r Schmidt values in decreasing order, such

that only $O(rN)$ physical resources (number of MZIs) and $O(rN)$ iterations are in principle required, which can be a substantial improvement for high-dimensional systems with low Schmidt numbers, as compared to the worst-case $O(N^2)$ requirement using traditional Schmidt decomposition methods.

If single photons in either subspace are lost (e.g., absorbed or scattered), the input and output can mix with a vacuum state, which might result in errors in the power or coincidence measurements. In the SM, Section S3, we model such detection and insertion losses as coupling each output and input port to a reservoir. We find that output losses do not affect the optimization process and can be readily calibrated out by measuring the transmission matrix of the network (as is typically done in entanglement distribution experiments[67]). Nonuniform insertion losses at the input can distort the input state.[60,61] In that case, the coincidence optimization can still learn the correct SVD of the distorted input state traversing the network, while the sequential power optimization does not (nonetheless, in both cases, there is enough information to reconstruct the original state, if the transmission matrix is known). This problem can be alleviated by equalizing insertion losses, preventing distortions, and allowing both the power and coincidence optimizations to learn the SVD of the input quantum state. Large losses may, however, result in reducing the number of counts on the detector and slow down the training process. Other MZI mesh architectures may also alleviate the influence of losses and imperfections.[59,68] In general, we expect that well-established MZI calibration methods will be critical in mitigating the influence of these different loss mechanisms in practical experimental settings.[59] This robustness to single photon losses provides further motivation to investigate the performance of our method in experimentally relevant settings.

Analyzing and Processing Entanglement in Spontaneously Down-Converted Photon Pairs. We now investigate the performance of our method in the analysis of entangled photon pairs generated via SPDC. As noted in the previous section, our method is naturally suited for the analysis of spatial mode entanglement. To further generalize the applicability of our approach, we consider below the case of frequency bin entanglement. This concept could be readily generalized to other high-dimensional Hilbert spaces, e.g., correlations in spatial modes such as orbital angular momentum.[69–71] We further discuss in the SI, Section S5 how to generalize our approach to arbitrary degrees of freedom by using universal converters to spatial modes.[52,72] The proposed experimental setup that we model is shown in Figure 3a. We consider a second-order nonlinear crystal pumped by a laser at frequency ω_p and spontaneously generating photon pairs at frequencies ω_s (signal) and ω_i (idler). The SPDC photons then go through an optional spectral filter to shape the joint spectral density (width σ_f) and a polarizing beam splitter to split the signal and idler beams. Gratings are then used to diffract spectral modes of the idler (signal) photons, occupying equidistant frequency bins centered around $\omega_{i(s),j} = \omega_{i(s),0} + j\Omega$, into the corresponding spatial input modes x_j (which couple to the network with a grating coupler). The frequency bins, now occupying different spatial modes, are then shifted to a common frequency $\omega_{i(s),0}$ (see SM Section S5). This can be done by an array of (on-chip) electro-optic frequency shifters[62,73–75] driven by corresponding Ω harmonics. (Similarly, for analyzing orbital

Figure 3. Automatic entanglement analysis of spontaneous parametric down-converted (SPDC) photons. (a) Proposed experimental setup to automatically analyze the entanglement of photon pairs generated via nondegenerate SPDC. A laser at frequency ω_p is pumping a second-order nonlinear crystal spontaneously generating entangled photon pairs at idler and signal frequencies (ω_i, ω_s), separated by a polarization beam splitter (PBS). Different frequency components are routed to different input ports of two self-configuring networks (SCNs) denoted A (ω_i) and B (ω_s). The SCN performs sequential coincidence counts maximization to automatically perform the Schmidt decomposition of the photon pair. (b–d) Input joint spectral amplitude (JSA). (e–g) Entanglement analysis with BSCN. S denotes the von Neumann entropy. (b,e) Numerical results for an unfiltered SPDC experiment ($\sigma_f \rightarrow \infty$, as defined in SM, Section S4). (c,f) Same as (b,e) but with a filter applied to the signal and idler modes ($\sigma_f = 0.09$). (d,g) Same as (b,e) but with a filter ($\sigma_f = 0.2$) and group velocity mismatch (GVM) corrections. All frequencies are normalized to the frequency range of interest: the pump bandwidth is $\sigma = 0.1$ for (b,c) and $\sigma = 0.5$ for (d).

angular momentum entanglement, the gratings and frequency shifters can be replaced by an off-chip spatial mode sorter[76,77] that converts orbital angular momentum modes into deflected Gaussian modes, which then couple to the chip.)

In the absence of insertion and detection losses, and spectral mixing by the gratings and frequency shifters (as shown in SM Section S3 and discussed above, the BSCN is robust to such imperfections), the resulting input state to the BSCN is

$$|\psi_{in}\rangle = \sum_{j,k} f(\nu_{s,j}, \nu_{i,k})|x_j\rangle_A |x_k\rangle_B \tag{6}$$

where $f(\nu_s, \nu_i)$ is the JSA of the photon pair at frequency (ν_s, ν_i), and $\nu_{s,j} = \omega_{s,j} - \omega_{s,0}$ and $\nu_{i,k} = \omega_{i,k} - \omega_{i,0}$ correspond to the discrete frequency bins around the central frequencies. The
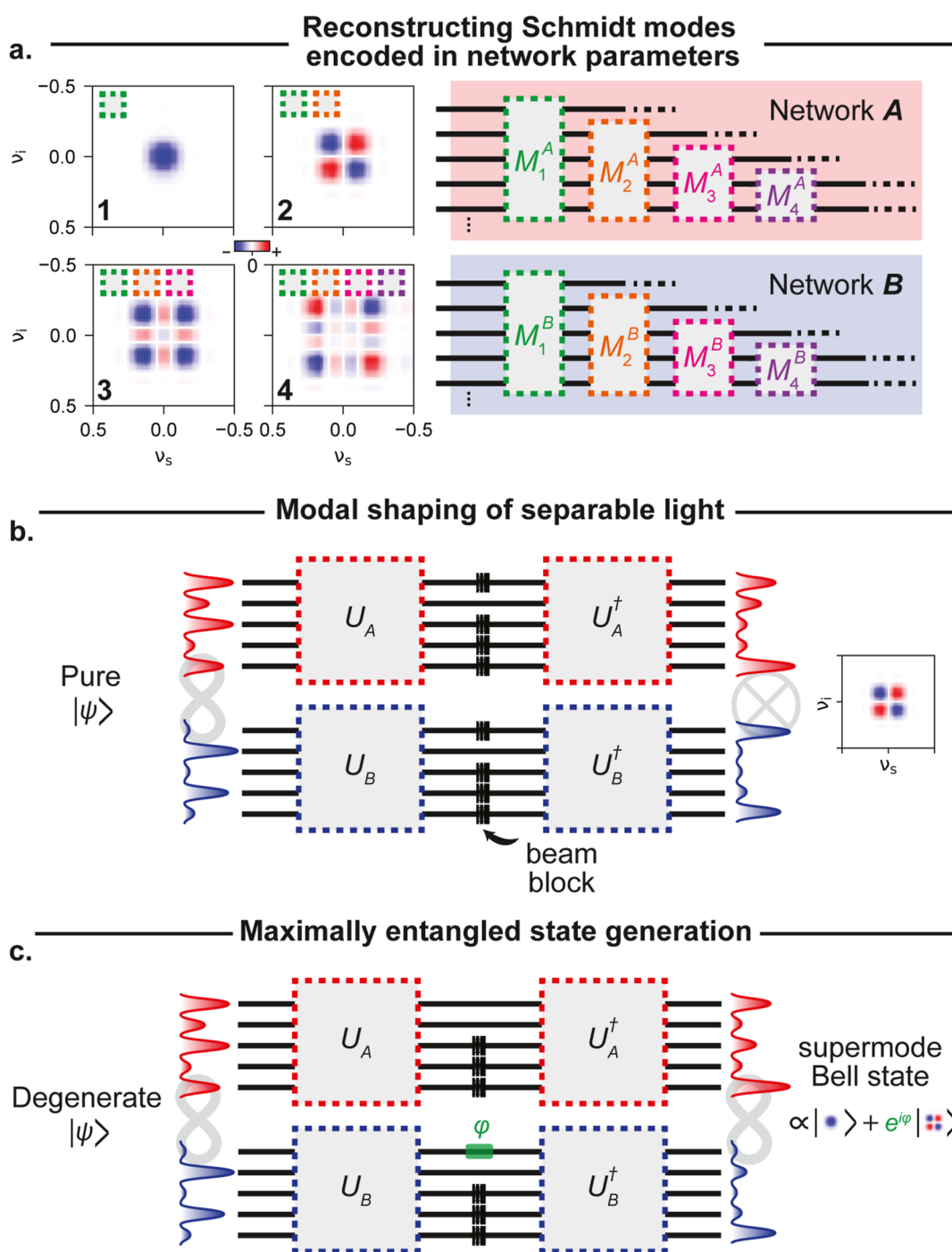
JSA can be controlled by shaping the incident pump spectrum,[78,79] the nonlinear crystal poling pattern,[19,23,24] dispersion engineering,[80,81] or adiabatic frequency conversion.[82] Below, we focus on the ubiquitous scenarios of spectral filtering and group velocity mismatch between the pump, signal, and idler (Figure 3d,g). Further details on our experimental model can be found in SM, Section S4.

Several phase-matching settings are shown in Figure 3b–d, as well as the BSCN output after convergence, in Figure 3e–g. In all cases, the BSCN learns the Schmidt decomposition of the input state, and we can use the average coincidence counts to calculate the input state's von Neumann entropy (with negligible error compared to the ground truth value <1%). The addition of a spectral filter in Figure 3c,f reduces the entanglement by removing spectral components of the photon pair, namely, making the state "more separable". In general, group velocity mismatch is present (Figure 3d,g), resulting in anticorrelated side lobes in the JSA. Several methods have been proposed to further shape the joint spectral density with engineered crystals[18] and pumps,[83] and the BSCN could be also applied to perform modal analysis of entanglement in these cases as well. We note that the experimental proposal from Figure 3 might be generalized to a fully integrated setup. This could be achieved by leveraging on-chip biphoton sources[84,85] and would avoid coupling losses due to grating couplers.

A distinctive feature of our method is that the Schmidt modes (including their phases, see SM, Section S2C) are directly encoded into the parameters of the network after it has converged. Specifically, the k-th Schmidt mode is encoded in the network parameters (e.g., the phase shifts for various waveguide segments of MZIs) of layers 1, ..., k of both networks A and B. We can therefore reconstruct the Schmidt modes (of the SPDC example from Figure 3d), as shown in Figure 4a. The self-configuring layers used for the reconstruction of each mode are indicated with dashed square boxes in each panel.

By automatically performing modal decomposition of the entanglement structure of the input state, the BSCN offers other possibilities in the modal shaping and generation of entanglement states. Namely, by blocking all output ports except the ones corresponding to a given biphoton mode, and using them as inputs for a pair of inverse networks (or even by reflecting them back through the output ports of the original networks), one can generate separable states with known shape (e.g., in spectral or spatial domain), as shown in Figure 4b. Additionally, if one inputs a degenerate quantum state (such that $\lambda_1 \approx \lambda_2$, as can be done with broadband phase-matching[86] or engineered nonlinear crystals[18]), a "supermode Bell state" can be generated by considering the output of the first two ports of both networks (see Figure 4c): $|\psi_{out}\rangle \propto \lambda_1(|x_1\rangle_A |x_1\rangle_B + e^{i\varphi}|x_2\rangle_A |x_2\rangle_B)$, where an additional phase φ can be imparted by a phase shifter on one of the output ports.

Entanglement Distribution through Scattering Media with BSCN. By shaping the modal composition of entangled states, our approach can also be applied to quantum communication protocols. One famous example is that of quantum teleportation[4] between two agents Alice (A) and Bob (B), where a Bell state is provided by a third-party source C (see Figure 5). A successful implementation of quantum teleportation entails the distribution of entanglement between the two parties A and B, or, in other words, the communication of each photon of the Bell state to each of the two parties. In
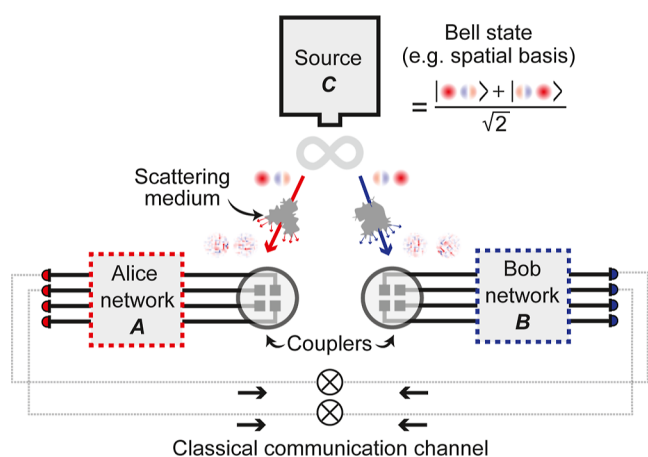
Figure 4. Schmidt mode reconstruction and entangled light processing with bipartite self-configuring optics. (a) Left: First four Schmidt modes reconstructed from BSCN parameters in the SPDC example of Figure 3d,g. Right: BSCN architecture for reference, where each self-configuring layer is highlighted in a different color. The self-configuring layers used to reconstruct the Schmidt modes on the left are represented by the number and color of gray squares as insets. (b) Once trained, BSCN can be used to generate separable light with a given modal shape by blocking all output ports except the two ports corresponding to that mode index (in networks A and B) and feeding them as input to networks applying the inverse transformation. (c) If trained on a highly degenerate input state (such that two singular values are approximately equal), BSCN can also be used to generate supermode Bell states (by blocking all output ports except the four ports corresponding to degenerate singular values in each network). An additional phase shifter can be added on one of the output ports to control the relative phase between the two terms of the pair.

real-life settings, this communication may experience scattering and mode mixing through different communication channels (e.g., due to random scattering). The scattering of quantum light through complex media is an active field of research,[67] with immediate applications to quantum communication and entanglement distribution protocols through scattering chan-nels such as turbulent atmosphere and multimode fibers. Conventional schemes compensate for the scattering through adaptive wavefront shaping of the photon pairs by character-izing the channel using an auxiliary laser at or near the same photon frequency[87−90] or even the pump laser used to generate the photons.[91]

Figure 5. Entanglement distribution through scattering media with BSCN. Proposed setup for quantum teleportation through scattering media with BSCN. A source C is generating Bell states sent to Alice (A) and Bob (B) who analyze their single photon with their own SCN. A classical communication channel between the two allows them to perform coincidence measurements.

The BSCN offers an alternative approach based on automatic Schmidt decomposition via sequential coincidence optimization. Specifically, if both Alice and Bob possess a SCN that they use to process the photon they receive and perform the Schmidt learning method described in this work, they can learn the basis in which Alice should perform measurement to teleport her state to Bob. To do so, a classical communication channel is necessary between Alice and Bob, but there is no need to perform any characterizations of the communication channels between the source and either Alice or Bob. More generally, the BSCN allows us to undo the influence of random scattering when measuring multimode entangled states. A formal derivation of this communication protocol is provided in the SM, Section S8.

In fact, in this protocol, the BSCN finds the effective communication modes[55,60] between Alice and Bob. This idea can therefore be generalized to the Klyshko configuration,[92] which replaces one of the photon detectors (say, Alice's) by a classical input laser beam to characterize the effective scattering channel between Alice, the source, and Bob. Characterizing the communication channel in this manner to configure the BSCN could boost the convergence speed and detection bandwidth of the protocol, which can be critical for entanglement distribution in rapidly fluctuating media.

■ DISCUSSION AND CONCLUSION

We further discuss potential applications of our method and experimental considerations for their realization.

Our methods could be applied to entanglement analysis in other quantum systems, such as temporal entanglement in atom-photon coupling[93] and macroscopic quantum states of light, such as bright squeezed vacuum.[26,38] In both cases, multimodal entanglement over temporal, spatial, or spectral degrees of freedom can be described on the Schmidt basis, which reveals the fundamental mechanisms of entanglement generation. Many of these systems, including photon pairs from SPDC, rely on several control parameters of light or matter that can be dynamically optimized to shape or maximize entanglement. Since the BSCN automatically learns the Schmidt decomposition of the input state, it could also serve

as a form of feedback on the system's control parameters to learn their influence on the entanglement structure of the input state. In particular, well-established techniques for shaping photon pairs[18−21,23,24,80] are often sensitive to experimental parameters such as beam alignment, poling fabrication, and even temperature. Additional imperfections, such as partial phase control, may have consequences on the accessible range of Schmidt modes, as is known from analogue theories in complex scattering medium.[94] Our proposal could allow for robustness and tunability even in the presence of experimental imperfections.

The automatic learning of the input state's Schmidt decomposition requires a pure input state of the network $|\psi_{in}\rangle$. Several sources of noise and imperfections may result in impurities of the quantum state. First, stochastic losses through the network yield a mixture of pure states with different photon numbers. With the above-mentioned loss model, we show that postselection on a given number state (e.g., by performing coincidence or single photon counts) mitigates the influence of this impurity on the performance of our algorithm (see SM, Section S3). Second, the input state might be mixed with other (random) states, resulting in a statistical mixture. In general, this would result in the emergence of cross-coincidence counts between output ports $|x_j\rangle_A$ and $|x_k\rangle_B$, where $j \neq k$ after diagonalization of the reduced density matrices performed by the BSCN (see SM, Section S6). Practically, this means that BSCN might also be used to "detect" impurities in the input quantum state in this more general setting.

Our proposal provides a high-dimensional (two-qudit) photonic-hardware implementation of variational quantum singular value decomposition circuits[95,96] which decompose bipartite entanglement of general multiple-qubit states. As a future direction, it will be interesting to generalize our architecture to bipartite entangled states of more than two photons, allowing for multiple-qudit variational quantum singular value decomposition circuits.

In conclusion, we have presented a general and versatile method to automatically analyze the entanglement of a multimode quantum optical state. Our method relies on a variational definition of the Schmidt decomposition performed by a BSCN. The methods presented in this work could be applied to a wide range of quantum optical systems, where the engineering and shaping of entanglement play an essential role.

■ ASSOCIATED CONTENT

Data Availability Statement

The data and codes that support the plots within this paper and other findings of this study are available from the corresponding authors upon reasonable request. Correspondence and requests for materials should be addressed to C.R.-C. (chrc@stanford.edu) and A.K. (karnieli@stanford.edu).

ⓈI Supporting Information

The Supporting Information is available free of charge at https://pubs.acs.org/doi/10.1021/acsphotonics.5c00813.

> Background on Schmidt decomposition, sequential optimization algorithms: power-based and coincidence-based methods for self-configuring optical Schmidt decomposition, influence of losses: impact on Schmidt mode recovery and optimization, entanglement analysis: application to SPDC photons and measurement of entanglement, frequency-bin basis and generalizations:

extension to frequency modes and other degrees of freedom, impurity characterization: assessment of mixed-state contributions via cross-coincidence detection, convergence: formal proof for the optimization algorithms, and communication protocol: implementation details using BSCN (PDF)

■ AUTHOR INFORMATION

Corresponding Authors

Charles Roques-Carmes − *E. L. Ginzton Laboratory, Stanford University, Stanford, California 94305, United States;* ⊙ orcid.org/0000-0002-1168-5944; Email: chrc@stanford.edu

Aviv Karnieli − *E. L. Ginzton Laboratory, Stanford University, Stanford, California 94305, United States;* ⊙ orcid.org/0000-0002-4056-4455; Email: karnieli@stanford.edu

Shanhui Fan − *E. L. Ginzton Laboratory, Stanford University, Stanford, California 94305, United States;* ⊙ orcid.org/0000-0002-0081-9732; Email: shanhui@stanford.edu

Author

David A. B. Miller − *E. L. Ginzton Laboratory, Stanford University, Stanford, California 94305, United States*

Complete contact information is available at:
https://pubs.acs.org/10.1021/acsphotonics.5c00813

■ REFERENCES

(1) Horodecki, R.; Horodecki, P.; Horodecki, M.; Horodecki, K. Quantum entanglement. *Rev. Mod. Phys.* **2009**, *81* (2), 865.

(2) Shor, P. W. Polynomial-time algorithms for prime factorization and discrete logarithms on a quantum computer. *SIAM Rev.* **1999**, *41* (2), 303−332.

(3) Yin, J.; Li, Y.-H.; Liao, S.-K.; Yang, M.; Cao, Y.; Zhang, L.; Ren, J.-G.; Cai, W.-Q.; Liu, W.-Y.; Li, S.-L.; et al. Entanglement-based secure quantum cryptography over 1,120 kilometres. *Nature* **2020**, *582* (7813), 501−505.

(4) Bouwmeester, D.; Pan, J.-W.; Mattle, K.; Eibl, M.; Weinfurter, H.; Zeilinger, A. Experimental quantum teleportation. *Nature* **1997**, *390* (6660), 575−579.

(5) Aspect, A.; Dalibard, J.; Roger, G. Experimental test of bell's inequalities using time-varying analyzers. *Phys. Rev. Lett.* **1982**, *49* (25), 1804.

(6) Gröblacher, S.; Paterek, T.; Kaltenbaek, R.; Brukner, C. ˇ.; Żukowski, M.; Aspelmeyer, M.; Zeilinger, A. An experimental test of non-local realism. *Nature* **2007**, *446* (7138), 871−875.

(7) Raimond, J.-M.; Brune, M.; Haroche, S. Manipulating quantum entanglement with atoms and photons in a cavity. *Rev. Mod. Phys.* **2001**, *73* (3), 565.

(8) O'brien, J. L.; Furusawa, A.; Vučković, J. Photonic quantum technologies. *Nat. Photonics* **2009**, *3* (12), 687−695.

(9) Wineland, D. J. Nobel lecture: Superposition, entanglement, and raising Schrödinger's cat. *Rev. Mod. Phys.* **2013**, *85* (3), 1103.

(10) Erhard, M.; Krenn, M.; Zeilinger, A. Advances in high-dimensional quantum entanglement. *Nat. Rev. Phys.* **2020**, *2* (7), 365−381.

(11) Carolan, J.; Harrold, C.; Sparrow, C.; Martín-López, E.; Russell, N. J.; Silverstone, J. W.; Shadbolt, P. J.; Matsuda, N.; Oguma, M.; Itoh, M.; et al. Universal linear optics. *Science* **2015**, *349* (6249), 711−716.

(12) Zhong, H.-S.; Wang, H.; Deng, Y.-H.; Chen, M.-C.; Peng, L.-C.; Luo, Y.-H.; Qin, J.; Wu, D.; Ding, X.; Hu, Y.; et al. Quantum computational advantage using photons. *Science* **2020**, *370* (6523), 1460−1463.

(13) Bogdanov, Y. I.; Chekhova, M.; Kulik, S.; Maslennikov, G.; Zhukov, A.; Oh, C.; Tey, M. Qutrit state engineering with biphotons. *Phys. Rev. Lett.* **2004**, *93* (23), 230503.

(14) Zhang, Z.; You, C.; Magaña-Loaiza, O. S.; Fickler, R.; León-Montiel, R. d. J.; Torres, J. P.; Humble, T. S.; Liu, S.; Xia, Y.; Zhuang, Q. Entanglement-based quantum information technology: a tutorial. *Adv. Opt. Photonics* **2024**, *16* (1), 60−162.

(15) Burlakov, A.; Chekhova, M.; Karabutova, O.; Klyshko, D.; Kulik, S. Polarization state of a biphoton: Quantum ternary logic. *Phys. Rev. A* **1999**, *60* (6), R4209.

(16) Fedorov, M.; Efremov, M.; Volkov, P.; Moreva, E.; Straupe, S.; Kulik, S. Spontaneous parametric down-conversion: Anisotropical and anomalously strong narrowing of biphoton momentum correlation distributions. *Phys. Rev. A* **2008**, *77* (3), 032336.

(17) Fedorov, M.; Volkov, P.; Mikhailova, J. M.; Straupe, S.; Kulik, S. Entanglement of biphoton states: qutrits and ququarts. *New J. Phys.* **2011**, *13* (8), 083004.

(18) Hurvitz, I.; Karnieli, A.; Arie, A. Frequency-domain engineering of bright squeezed vacuum for continuous-variable quantum information. *Opt. Express* **2023**, *31* (12), 20387−20397.

(19) Shukhin, A.; Hurvitz, I.; Trajtenberg-Mills, S.; Arie, A.; Eisenberg, H. Two-dimensional control of a biphoton joint spectrum. *Opt. Express* **2024**, *32* (6), 10158−10174.

(20) Dosseva, A.; Cincio, Ł.; Brańczyk, A. M. Shaping the joint spectrum of down-converted photons through optimized custom poling. *Phys. Rev. A* **2016**, *93* (1), 013801.

(21) Meyer-Scott, E.; Montaut, N.; Tiedau, J.; Sansoni, L.; Herrmann, H.; Bartley, T. J.; Silberhorn, C. Limits on the heralding efficiencies and spectral purities of spectrally filtered single photons from photon-pair sources. *Phys. Rev. A* **2017**, *95* (6), 061803.

(22) Graffitti, F.; Kelly-Massicotte, J.; Fedrizzi, A.; Brańczyk, A. M. Design considerations for high-purity heralded single-photon sources. *Phys. Rev. A* **2018**, *98* (5), 053811.

(23) Graffitti, F.; Barrow, P.; Pickston, A.; Brańczyk, A. M.; Fedrizzi, A. Direct generation of tailored pulse-mode entanglement. *Phys. Rev. Lett.* **2020**, *124* (5), 053603.

(24) Morrison, C. L.; Graffitti, F.; Barrow, P.; Pickston, A.; Ho, J.; Fedrizzi, A. Frequency-bin entanglement from domain-engineered down-conversion. *APL Photonics* **2022**, *7* (6), 066102.

(25) Fedorov, M.; Miklin, N. Schmidt modes and entanglement. *Contemp. Phys.* **2014**, *55* (2), 94−109.

(26) Sharapova, P.; Pérez, A. M.; Tikhonova, O. V.; Chekhova, M. V. Schmidt modes in the angular spectrum of bright squeezed vacuum. *Phys. Rev. A* **2015**, *91* (4), 043816.

(27) Just, F.; Cavanna, A.; Chekhova, M. V.; Leuchs, G. Transverse entanglement of biphotons. *New J. Phys.* **2013**, *15* (8), 083015.

(28) Amooei, M.; Kulkarni, G.; Upham, J.; Boyd, R. W. Efficient characterization of spatial Schmidt modes of multiphoton entangled states produced from high-gain parametric down-conversion. *Phys. Rev. A* **2025**, *111*, 023714.

(29) Bhattacharjee, A.; Meher, N.; Jha, A. K. Measurement of two-photon position−momentum Einstein−Podolsky−Rosen correlations through single-photon intensity measurements. *New J. Phys.* **2022**, *24* (5), 053033.

(30) Averchenko, V. A.; Frascella, G.; Kalash, M.; Cavanna, A.; Chekhova, M. V. Reconstructing two-dimensional spatial modes for classical and quantum light. *Phys. Rev. A* **2020**, *102* (5), 053725.

(31) Kulkarni, G.; Taneja, L.; Aarav, S.; Jha, A. K. Angular Schmidt spectrum of entangled photons: derivation of an exact formula and experimental characterization for noncollinear phase matching. *Phys. Rev. A* **2018**, *97* (6), 063846.

(32) Kulkarni, G.; Rioux, J.; Braverman, B.; Chekhova, M. V.; Boyd, R. W. Classical model of spontaneous parametric down-conversion. *Phys. Rev. Res.* **2022**, *4* (3), 033098.

(33) Dixon, P. B.; Howland, G. A.; Schneeloch, J.; Howell, J. C. Quantum mutual information capacity for high-dimensional entangled states. *Phys. Rev. Lett.* **2012**, *108* (14), 143603.

(34) Luo, Y.-H.; Zhong, H.-S.; Erhard, M.; Wang, X.-L.; Peng, L.-C.; Krenn, M.; Jiang, X.; Li, L.; Liu, N.-L.; Lu, C.-Y.; et al. Quantum teleportation in high dimensions. *Phys. Rev. Lett.* **2019**, *123* (7), 070505.

(35) Sit, A.; Bouchard, F.; Fickler, R.; Gagnon-Bischoff, J.; Larocque, H.; Heshami, K.; Elser, D.; Peuntinger, C.; Günthner, K.; Heim, B.; et al. High-dimensional intracity quantum cryptography with structured photons. *Optica* **2017**, *4* (9), 1006−1010.

(36) Asban, S.; Dorfman, K. E.; Mukamel, S. Quantum phase-sensitive diffraction and imaging using entangled photons. *Proc. Natl. Acad. Sci. U.S.A.* **2019**, *116* (24), 11673−11678.

(37) Fuenzalida, J.; Hochrainer, A.; Lemos, G. B.; Ortega, E. A.; Lapkiewicz, R.; Lahiri, M.; Zeilinger, A. Resolution of quantum imaging with undetected photons. *Quantum* **2022**, *6*, 646.

(38) Sharapova, P.; Tikhonova, O.; Lemieux, S.; Boyd, R.; Chekhova, M. Bright squeezed vacuum in a nonlinear interferometer: Frequency and temporal Schmidt-mode description. *Phys. Rev. A* **2018**, *97* (5), 053827.

(39) Straupe, S.; Ivanov, D.; Kalinkin, A.; Bobrov, I.; Kulik, S. Angular Schmidt modes in spontaneous parametric down-conversion. *Phys. Rev. A* **2011**, *83* (6), 060302.

(40) Law, C.; Eberly, J. Analysis and interpretation of high transverse entanglement in optical parametric down conversion. *Phys. Rev. Lett.* **2004**, *92* (12), 127903.

(41) Jha, A. K.; Agarwal, G. S.; Boyd, R. W. Partial angular coherence and the angular Schmidt spectrum of entangled two-photon fields. *Phys. Rev. A: At., Mol, Opt. Phys.* **2011**, *84* (6), 063847.

(42) Van Exter, M.; Aiello, A.; Oemrawsingh, S.; Nienhuis, G.; Woerdman, J. Effect of spatial filtering on the Schmidt decomposition of entangled photons. *Phys. Rev. A: At., Mol., Opt. Phys.* **2006**, *74* (1), 012309.

(43) Miatto, F. M.; di Lorenzo Pires, H.; Barnett, S. M.; van Exter, M. P. Spatial Schmidt modes generated in parametric down-conversion. *Eur. Phys. J. D* **2012**, *66*, 263.

(44) Bogaerts, W.; Pérez, D.; Capmany, J.; Miller, D. A. B.; Poon, J.; Englund, D.; Morichetti, F.; Melloni, A. Programmable photonic circuits. *Nature* **2020**, *586* (7828), 207−216.

(45) Harris, N. C.; Carolan, J.; Bunandar, D.; Prabhu, M.; Hochberg, M.; Baehr-Jones, T.; Fanto, M. L.; Smith, A. M.; Tison, C. C.; Alsing, P. M.; et al. Linear programmable nanophotonic processors. *Optica* **2018**, *5* (12), 1623−1631.

(46) Sibson, P.; Erven, C.; Godfrey, M.; Miki, S.; Yamashita, T.; Fujiwara, M.; Sasaki, M.; Terai, H.; Tanner, M. G.; Natarajan, C. M.; et al. Chip-based quantum key distribution. *Nat. Commun.* **2017**, *8* (1), 13984.

(47) Peruzzo, A.; McClean, J.; Shadbolt, P.; Yung, M.-H.; Zhou, X.-Q.; Love, P. J.; Aspuru-Guzik, A.; O'brien, J. L. A variational eigenvalue solver on a photonic quantum processor. *Nat. Commun.* **2014**, *5* (1), 4213.

(48) Carolan, J.; Mohseni, M.; Olson, J. P.; Prabhu, M.; Chen, C.; Bunandar, D.; Niu, M. Y.; Harris, N. C.; Wong, F. N.; Hochberg, M.; et al. Variational quantum unsampling on a quantum photonic processor. *Nat. Phys.* **2020**, *16* (3), 322−327.

(49) Matthews, J. C.; Politi, A.; Stefanov, A.; O'brien, J. L. Manipulation of multiphoton entanglement in waveguide quantum circuits. *Nat. Photonics* **2009**, *3* (6), 346−350.

(50) Wang, J.; Paesani, S.; Ding, Y.; Santagati, R.; Skrzypczyk, P.; Salavrakos, A.; Tura, J.; Augusiak, R.; Mančinska, L.; Bacco, D.; et al. Multidimensional quantum entanglement with large-scale integrated optics. *Science* **2018**, *360* (6386), 285−291.

(51) Harris, N. C.; Steinbrecher, G. R.; Prabhu, M.; Lahini, Y.; Mower, J.; Bunandar, D.; Chen, C.; Wong, F. N.; Baehr-Jones, T.; Hochberg, M.; et al. Quantum transport simulations in a programmable nanophotonic processor. *Nat. Photonics* **2017**, *11* (7), 447−452.

(52) Miller, D. A. B. Self-configuring universal linear optical component. *Photon. Res.* **2013**, *1* (1), 1−15.

(53) Miller, D. A. B. Self-aligning universal beam coupler. *Opt. Express* **2013**, *21* (5), 6360−6370.

(54) Miller, D. A. Waves, modes, communications, and optics: a tutorial. *Adv. Opt. Photonics* **2019**, *11* (3), 679−825.

(55) SeyedinNavadeh, S.; Milanizadeh, M.; Zanetto, F.; Ferrari, G.; Sampietro, M.; Sorel, M.; Miller, D. A. B.; Melloni, A.; Morichetti, F. Determining the optimal communication channels of arbitrary optical systems using integrated photonic processors. *Nat. Photonics* **2023**, *18*, 149−155.

(56) Miller, D. A. B. Analyzing and generating multimode optical fields using self-configuring networks. *Optica* **2020**, *7*, 794−801.

(57) Milanizadeh, M.; Toso, F.; Ferrari, G.; Jonuzi, T.; Miller, D. A. B.; Melloni, A.; Morichetti, F. Coherent self-control of free-space optical beams with integrated silicon photonic meshes. *Photon. Res.* **2021**, *9* (11), 2196−2204.

(58) Pai, S.; Sun, Z.; Hughes, T. W.; Park, T.; Bartlett, B.; Williamson, I. A.; Minkov, M.; Milanizadeh, M.; Abebe, N.; Morichetti, F.; et al. Experimentally realized in situ backpropagation for deep learning in photonic neural networks. *Science* **2023**, *380* (6643), 398−404.

(59) Miller, D. A. B. Perfect optics with imperfect components. *Optica* **2015**, *2* (8), 747−750.

(60) Miller, D. A. B. Establishing optimal wave communication channels automatically. *J. Lightwave Technol.* **2013**, *31* (24), 3987−3994.

(61) Roques-Carmes, C.; Fan, S.; Miller, D. A. Measuring, processing, and generating partially coherent light with self-configuring optics. *Light: Sci. Appl.* **2024**, *13* (1), 260.

(62) Lu, H.-H.; Liscidini, M.; Gaeta, A. L.; Weiner, A. M.; Lukens, J. M. Frequency-bin photonic quantum information. *Optica* **2023**, *10* (12), 1655−1671.

(63) Nielsen, M. A.; Chuang, I. L. *Quantum Computation and Quantum Information*; Cambridge University Press, 2010.

(64) Hughes, T. W.; Minkov, M.; Shi, Y.; Fan, S. Training of photonic neural networks through in situ backpropagation and gradient measurement. *Optica* **2018**, *5* (7), 864−871.

(65) KingmaBa, D. P. J. Adam: A method for stochastic optimization. *arXiv* **2014**, arXiv:1412.6980.

(66) Du, S. S.; Jin, C.; Lee, J. D.; Jordan, M. I.; Singh, A.; Poczos, B. Gradient descent can take exponential time to escape saddle points. *Advances in Neural Information Processing Systems*; NIPS, 2017; Vol. 30.

(67) Lib, O.; Bromberg, Y. Quantum light in complex media and its applications. *Nat. Phys.* **2022**, *18* (9), 986−993.

(68) Burgwal, R.; Clements, W. R.; Smith, D. H.; Gates, J. C.; Kolthammer, W. S.; Renema, J. J.; Walmsley, I. A. Using an imperfect photonic network to implement random unitaries. *Opt. Express* **2017**, *25* (23), 28236−28245.

(69) Mair, A.; Vaziri, A.; Weihs, G.; Zeilinger, A. Entanglement of the orbital angular momentum states of photons. *Nature* **2001**, *412* (6844), 313−316.

(70) Erhard, M.; Fickler, R.; Krenn, M.; Zeilinger, A. Twisted photons: new quantum perspectives in high dimensions. *Light: Sci. Appl.* **2018**, *7* (3), 17146.

(71) Kovlakov, E.; Straupe, S.; Kulik, S. Quantum state engineering with twisted photons via adaptive shaping of the pump beam. *Phys. Rev. A* **2018**, *98* (6), 060301.

(72) Miller, D. A.; Roques-Carmes, C.; Valdez, C. G.; Kroo, A. R.; Vlk, M.; Fan, S.; Solgaard, O. Universal programmable and self-configuring optical filter. *arXiv* **2025**, arXiv:2501.11811.

(73) Hu, Y.; Yu, M.; Zhu, D.; Sinclair, N.; Shams-Ansari, A.; Shao, L.; Holzgrafe, J.; Puma, E.; Zhang, M.; Lončar, M. On-chip electro-optic frequency shifters and beam splitters. *Nature* **2021**, *599* (7886), 587−593.

(74) Zhu, D.; Chen, C.; Yu, M.; Shao, L.; Hu, Y.; Xin, C.; Yeh, M.; Ghosh, S.; He, L.; Reimer, C.; et al. Spectral control of nonclassical light pulses using an integrated thin-film lithium niobate modulator. *Light: Sci. Appl.* **2022**, *11* (1), 327.

(75) Lingaraju, N. B.; Lu, H.-H.; Leaird, D. E.; Estrella, S.; Lukens, J. M.; Weiner, A. M. Bell state analyzer for spectrally distinct photons. *Optica* **2022**, *9* (3), 280−283.

(76) Fickler, R.; Lapkiewicz, R.; Huber, M.; Lavery, M. P.; Padgett, M. J.; Zeilinger, A. Interface between path and orbital angular momentum entanglement for high-dimensional photonic quantum information. *Nat. Commun.* **2014**, *5* (1), 4502.

(77) Lightman, S.; Hurvitz, G.; Gvishi, R.; Arie, A. Miniature wide-spectrum mode sorter for vortex beams produced by 3d laser printing. *Optica* **2017**, *4* (6), 605−610.

(78) Werner, M.; Raymer, M.; Beck, M.; Drummond, P. Ultrashort pulsed squeezing by optical parametric amplification. *Phys. Rev. A* **1995**, *52* (5), 4202.

(79) Arzani, F.; Fabre, C.; Treps, N. Versatile engineering of multimode squeezed states by optimizing the pump spectral profile in spontaneous parametric down-conversion. *Phys. Rev. A* **2018**, *97* (3), 033808.

(80) U'Ren, A. B.; Silberhorn, C.; Erdmann, R.; Banaszek, K.; Grice, W. P.; Walmsley, I. A.; Raymer, M. G. Generation of pure-state single-photon wavepackets by conditional preparation based on spontaneous parametric downconversion. *arXiv* **2006**, quant-ph/0611019.

(81) Christ, A.; Fedrizzi, A.; Hübel, H.; Jennewein, T.; Silberhorn, C. "Chapter 11—parametric down-conversion," in Single-Photon Generation and Detection. *Experimental Methods in the Physical Sciences*; Migdall, A., Polyakov, S. V., Fan, J., Bienfang, J. C., Eds.; Academic Press, 2013; Vol. *45*, pp 351−410.

(82) Presutti, F.; Wright, L. G.; Ma, S.-Y.; Wang, T.; Malia, B. K.; Onodera, T.; McMahon, P. L. Highly multimode visible squeezed light with programmable spectral correlations through broadband up-conversion. *arXiv* **2024**, arXiv:2401.06119.

(83) Boucher, P.; Defienne, H.; Gigan, S. Engineering spatial correlations of entangled photon pairs by pump beam shaping. *Opt. Lett.* **2021**, *46* (17), 4200−4203.

(84) Luo, R.; Jiang, H.; Rogers, S.; Liang, H.; He, Y.; Lin, Q. On-chip second-harmonic generation and broadband parametric down-conversion in a lithium niobate microresonator. *Opt. Express* **2017**, *25* (20), 24531−24539.

(85) Chapman, R. J.; Kuttner, T.; Kellner, J.; Sabatti, A.; Maeder, A.; Finco, G.; Kaufmann, F.; Grange, R. On-chip quantum interference between independent lithium niobate-on-insulator photon-pair sources. *arXiv* **2024**, arXiv:2404.08378.

(86) Zielnicki, K.; Garay-Palmett, K.; Cruz-Delgado, D.; Cruz-Ramirez, H.; O'Boyle, M. F.; Fang, B.; Lorenz, V. O.; U'Ren, A. B.; Kwiat, P. G. Joint spectral characterization of photon-pair sources. *J. Mod. Opt.* **2018**, *65* (10), 1141−1160.

(87) Defienne, H.; Barbieri, M.; Walmsley, I. A.; Smith, B. J.; Gigan, S. Two-photon quantum walk in a multimode fiber. *Sci. Adv.* **2016**, *2* (1), No. e1501054.

(88) Defienne, H.; Reichert, M.; Fleischer, J. W. Adaptive quantum optics with spatially entangled photon pairs. *Phys. Rev. Lett.* **2018**, *121* (23), 233601.

(89) Wolterink, T. A.; Uppu, R.; Ctistis, G.; Vos, W. L.; Boller, K.-J.; Pinkse, P. W. Programmable two-photon quantum interference in 10 3 channels in opaque scattering media. *Phys. Rev. A* **2016**, *93* (5), 053817.

(90) Cao, Y.; Li, Y.-H.; Yang, K.-X.; Jiang, Y.-F.; Li, S.-L.; Hu, X.-L.; Abulizi, M.; Li, C.-L.; Zhang, W.; Sun, Q.-C.; et al. Long-distance free-space measurement-device-independent quantum key distribution. *Phys. Rev. Lett.* **2020**, *125* (26), 260503.

(91) Lib, O.; Hasson, G.; Bromberg, Y. Real-time shaping of entangled photons by classical control and feedback. *Sci. Adv.* **2020**, *6* (37), No. eabb6298.

(92) Shekel, R.; Lib, O.; Bromberg, Y. Shaping entangled photons through arbitrary scattering media using an advanced wave beacon. *Opt. Quant.* **2024**, *2* (5), 303−309.

(93) Bogdanov, A. Y.; Bogdanov, Y. I.; Valiev, K. Schmidt modes and entanglement in continuous-variable quantum systems. *Russ. Microelectron.* **2006**, *35*, 7−20.

(94) Goetschy, A.; Stone, A. Filtering random matrices: the effect of incomplete channel control in multiple scattering. *Phys. Rev. Lett.* **2013**, *111* (6), 063901.

(95) Bravo-Prieto, C.; García-Martín, D.; Latorre, J. I. Quantum singular value decomposer. *Phys. Rev. A* **2020**, *101* (6), 062310.

(96) Wang, X.; Song, Z.; Wang, Y. Variational quantum singular value decomposition. *Quantum* **2021**, *5*, 483.

(97) Roques-Carmes, C.; Karnieli, A.; Miller, D. A.; Fan, S. Automated modal analysis of entanglement with bipartite self-configuring optics. *arXiv* **2024**, arXiv:2407.16849.